Heat and Mass Transfer

Shigeo Fujikawa
Takeru Yano
Masao Watanabe

Vapor-Liquid Interfaces, Bubbles and Droplets

Fundamentals and Applications

Springer

Heat and Mass Transfer

Series Editors: D. Mewes and F. Mayinger

For further volumes:
http://www.springer.com/series/4247

Shigeo Fujikawa · Takeru Yano ·
Masao Watanabe

Vapor-Liquid Interfaces, Bubbles and Droplets

Fundamentals and Applications

With 74 Figures

Springer

Prof. Shigeo Fujikawa
Hokkaido University
Dept. Mechanical & Space Engineering
Kita 13, Nishi 8
Sapporo
060-8628 Japan
fujikawa@eng.hokudai.ac.jp

Prof. Takeru Yano
Osaka University
Dept. Mechanical Engineering
Yamada-oka 2-1
Suita
565-0871 Japan
yano@mech.eng.osaka-u.ac.jp

Prof. Masao Watanabe
Hokkaido University
Dept. Mechanical & Space Engineering
Kita 13, Nishi 8
Sapporo
060-8628 Japan
masao.watanabe@eng.hokudai.ac.jp

ISSN 1860-4846 e-ISSN 1860-4854
ISBN 978-3-642-18037-8 e-ISBN 978-3-642-18038-5
DOI 10.1007/978-3-642-18038-5
Springer Heidelberg Dordrecht London New York

Library of Congress Control Number: 2011923076

Cover design: eStudio Calamar S.L., Heidelberg

Printed on acid-free paper

Springer is part of Springer Science+Business Media (www.springer.com)

Preface

This book is the outgrowth of work done over 30 years by the first author's group in the departments of Mechanical Engineering at Kyoto University, Mechanical Systems Engineering at Toyama Prefectural University, and Mechanical and Space Engineering at Hokkaido University. The work is concerned with basics of evaporation and condensation at the vapor–liquid interface where the bulk vapor phase and the bulk liquid phase of the same molecules coexist side by side. It focuses on physical understanding and mathematical description of interfacial phenomena in length scales ranging from a molecular size to a usual fluid-dynamic one, such as kinetic and fluid-dynamic boundary conditions including the evaporation and condensation coefficients, vapor pressure and surface tension for nanodroplets, and applications of fluid-dynamic boundary conditions to vapor bubble dynamics.

The meaning and significance of subjects to be discussed in the book are described in some detail in Chap. 1. It is needless to say that the evaporation and condensation are of paramount importance in various fields of engineering, physics, chemistry, meteorology, and oceanography. As examples of current topics related to the evaporation and condensation, we can refer to flows around aircraft in clouds, bubble formation in liquid fuels of rockets, vapor explosion in nuclear reactors and volcanoes, vapor bubble formation in LNG transport process, heterogeneous reaction on droplet and aerosol surfaces in the atmosphere, and so on. The crucial point in these problems can be attributed to boundary conditions at the interface for both the Boltzmann equation and the set of Navier–Stokes equations.

It was 2005 when a kinetic boundary condition (KBC) for the Boltzmann equation was formulated in a physically correct form. However, accurate values of the evaporation and condensation coefficients for any vapors have not been determined up to now, and therefore, we can not obtain still now physically correct solutions to these problems in theoretical and numerical ways. Historically, since the end of nineteen century, it has been known that the evaporation or condensation process requires the kinetic theory of gases for its analysis, and numerous investigations have been made by the kinetic approach, resulting in various fruits. However, in 1990s, it has been recognized that the kinetic theory of gases on the evaporation or condensation further needs microscopic information of molecules at the interface, e.g., correct KBC, exact values of the evaporation and condensation coefficients included in the KBC. Since then, molecular dynamics (MD) has received much

attention for simulation of the evaporation and condensation, and become a powerful tool to get microscopic information of the interface at atomic and molecular levels.

The authors have engaged in investigation of the evaporation and condensation at the interface by using their unique methodology based on MD, molecular gas dynamics, and shock wave. Using MD, they have made numerical simulations of molecular motions in domains consisting of the bulk vapor of argon, its liquid, and the planar interface between them, and thereby formulated the physically correct KBC. Furthermore, using shock waves, they have made experiments of condensation for methanol and water vapors in nanometer and microsecond scales and deduced values of the evaporation and condensation coefficients of these materials by the aid of the polyatomic version of the Gaussian–BGK Boltzmann equation, a governing equation in molecular gas dynamics.

The authors try to describe contents dealt with in this book as precisely as possible by restricting them to only their own work and to connect tightly them ranging from the microscopic to macroscopic scales. The evaporation or condensation phenomenon in the three space domains with utterly different length scales is analyzed by means of MD, the Gaussian–BGK Boltzmann equation, and the set of Navier–Stokes equations. Matching methods among the domains or the different governing equations are presented, and the reasonable matching between the microscopic and macroscopic scales is carried out to give the closed forms of the boundary conditions for both the Gaussian–BGK Boltzmann equation and the set of Navier–Stokes equations. A set of boundary conditions for the latter is applied to dynamics of a single vapor bubble in liquids as an application.

However, the authors must say that they had to restrict the problems on the boundary conditions and the evaporation and condensation coefficients to only a single-component vapor–liquid two-phase system and to weak evaporation or condensation because of overwhelming difficulties of the problems. A two-phase system consisting of a liquid and its vapor-noncondensable gas mixture is of importance in engineering applications. However, the derivation of physically correct kinetic and fluid-dynamic boundary conditions have not been accomplished and these are under development. Problems of such a system as well as strong evaporation or condensation are left as challenging subjects in the future.

The contributions to the chapters of this book are as follows: S. Fujikawa to Chaps. 1, 3, and 4; T. Yano to Chap. 2, and Appendices A and B; M. Watanabe to Chap. 5 and Appendix C. In writing this book, the authors are indebted to the following colleagues, their former Ph. D students; Prof. T. Ishiyama has contributed to Chap. 2 as his Ph. D work, Prof. K. Kobayashi to Chap. 3 as his Ph. D work, Dr. H. Yaguchi to Chap. 4 as his Ph. D work, and Drs S. Nakamura and M. Inaba partly to Chap. 3 as their Ph. D works. Without their contributions, this book might not have been born. The authors would also like to appreciate helps of Mr. Y. Nozaki, the technician in the first author's laboratory, for his fine technique in making the experimental apparatuses, Miss K. Itagaki for typing the manuscripts, and Mrs. Y. Fujikawa for making fine figures. Finally, the first author would like to express his deepest gratitude to Ministry of Education, Culture, Sports, Science

and Technology-Japan and Japan Society for the Promotion of Science for their continuous financial supports to his work on the evaporation and condensation over 30 years. Thanks to the financial supports, he could continue to do such a challenging work and accomplish his mission.

Hokkaido, Japan — Shigeo Fujikawa
Osaka, Japan — Takeru Yano
Hokkaido, Japan — Masao Watanabe
November, 2010

Contents

Chapter 1
Significance of Molecular and Fluid-Dynamic Approaches to Interface Phenomena

Abstract In this chapter, we introduce the fundamentals of the planar vapor–liquid interface between the bulk vapor phase and the bulk liquid phase of the same molecules, stressing some key concepts such as the transition layer between them, the Knudsen layer near the interface in the vapor region, and the boundary conditions at the interface for the Boltzmann equation and the set of Navier–Stokes equation. The reason why measurements of the evaporation and condensation coefficients in the boundary conditions have been difficult is clarified in a theoretical way. The significance of the matching among different governing dynamics, i.e., molecular dynamics (MD), molecular gas dynamics, and fluid dynamics for vapor flows near the interface is discussed to make relations among the following chapters clear.

1.1 Vapor–Liquid Interface and Kinetic Boundary Condition (KBC)

In fluid dynamics and molecular gas dynamics, boundary conditions are of paramount importance because they have relevance to the drag and lift exerted on bodies, and heat and mass transport across boundaries. Especially, the boundary conditions for the interface of the bulk vapor phase and the bulk liquid phase, at which evaporation or condensation occurs, involve some difficult problems [4, 11]. This is because the derivation of the boundary conditions requires detailed information of molecular phenomena at the interface, while the governing equations such as the set of Navier–Stokes equations in fluid dynamics and the Boltzmann equation in molecular gas dynamics can be derived from macroscopic and microscopic conservation laws, respectively.[1] In fact, recent studies on the boundary conditions at the interface have made significant progress by molecular dynamics (MD) simulations [8, 12, 16, 18, 24–26].

[1] The set of Navier–Stokes equations is summarized in Appendix B at the end of this book, and the Boltzmann equation is discussed in Sect. 2.3.

S. Fujikawa et al., *Vapor-Liquid Interfaces, Bubbles and Droplets*, Heat and Mass Transfer, DOI 10.1007/978-3-642-18038-5_1,

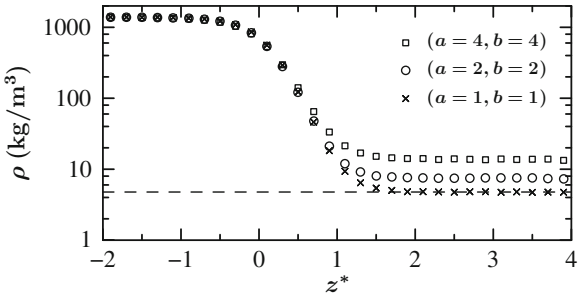

Fig. 1.1 Profiles of averaged density for argon at 85 K for some cases of (a, b). The dashed line denotes the saturated vapor density ($\rho_V = 4.59\,\mathrm{kg/m^3}$) at 85 K

When the evaporation or condensation exists in the interface, the vapor near the interface is in a nonequilibrium state in the sense that the velocity distribution function of molecules deviates from the Maxwellian (the Maxwell distribution function) prescribed by a temperature of the interface,[2] as will be discussed in Chap. 2. Let us first discuss the interface in a molecular level. Figure 1.1 shows profiles of averaged density ρ numerically obtained from MD simulations of argon [18]. As can be seen, the density continuously varies between the bulk liquid density ρ_L and the bulk vapor one ρ_V. The region where the density changes is called the (density) transition layer. The parameters a and b in the figure represent the deviation from the equilibrium state. The equilibrium state corresponds to $a = b = 1$, where $\rho_V = 4.59$ kg/m^3 (the saturated vapor density at 85 K), and $\rho_L = 1410$ kg/m^3. The vacuum evaporation state [16] is realized when $a = 0$. For $a = b = 2$ and 4, the vapors have higher densities than the saturated vapor density and negative velocities, which means net condensation states. Note that the compression factor $p/(\rho RT)$ is confirmed to be nearly unity in all cases, and hence the vapor can be regarded as an ideal gas. When the net condensation occurs, the interface moves toward the vapor phase. We therefore introduce a moving coordinate system [16], $z^* = [z - (Z_m - v_s t)]/\delta$ and $v_s = J_s/\rho_L$, where Z_m and δ are respectively the center position on a fixed coordinate and the 10–90 thickness (= 0.63 nm) of the transition layer, v_s is the speed of the moving coordinate, t is the time from the beginning of MD simulations, and J_s is the nonaveraged net mass flux across the interface.

We can see that the profiles are almost flat in the range $2 < z^* < 4$ of width 2δ in spite of the fact that the vapor is not in a local equilibrium state. This suggests that molecular collisions rarely happen there. In fact, the Knudsen number estimated by $\mathrm{Kn} = \ell/(2\delta) = 1/[\sqrt{2}\pi d_m^2(\rho/m)2\delta]$ is large (d_m is the diameter of a molecule, m

[2] According to molecular gas dynamics [29], an equilibrium state between the bulk vapor phase and the bulk liquid phase is defined as the state in which the velocity distribution function f of vapor molecules is given by the stationary Maxwellian in the coordinate system fixed at the vapor–liquid interface. Details are discussed in Sect. 2.3.1.

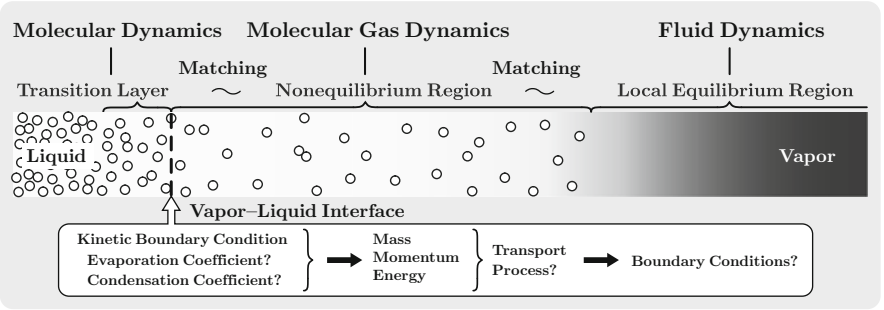

Fig. 1.2 The figure shows the whole space to be considered in this book. The space consists of the bulk liquid phase, the transition layer, the planar vapor–liquid interface, the Knudsen layer, and the bulk vapor phase of the same molecules in turn from the left-hand side. The space can be classified into three regions as follows: the transition region, the nonequilibrium region, and the local equilibrium region. The three regions obey different governing equations, i.e., molecular dynamics (MD) in the transition region, the Boltzmann equation in the nonequilibrium region, and the set of Navier–Stokes equations in the local equilibrium region. Open circles represent molecules, but they are not figured in the local equilibrium region because the fluid is assumed to be there continuum. The figure is symbolically depicted in largely different scales for the three regions

is the mass of a molecule, and ℓ is the mean free path of vapor molecules);[3] if d_m is replaced by the parameter σ ($= 0.341$ nm for argon) in the Lennard-Jones 12-6 potential,[4] Kn = 20.9, 13.5, and 7.3 for $a = b = 1, 2$, and 4, respectively. Since the thickness δ of the transition layer is regarded as zero in the kinetic theory and the change in the vapor condition in the range $2 < z^* < 4$ is negligible, the interface may be defined at an arbitrary position in this range. That is, the interface locates in the vapor phase adjacent to the vapor-side edge of the transition layer. We call it the kinetic interface. Hereafter, the kinetic interface will be called just the interface.

As shown in Fig. 1.2, there exists a nonequilibrium region in the neighborhood of the interface in the vapor region and it is called the Knudsen layer. The extent of this layer is of the order of the mean free path of vapor molecules. The nonequilibrium behavior of the vapor in the Knudsen layer plays an important role in the evaporation or condensation. Vapor flows accompanied with the evaporation or condensation across the interface should therefore be treated by molecular gas dynamics based on the Boltzmann equation [4, 28, 29]. The Boltzmann equation then requires the kinetic boundary condition (KBC) which prescribes the velocity distribution of molecules leaving the interface for the vapor phase.

When the evaporation or condensation across the interface is weak, the KBC is expressed by the product of the two-dimensional Gauss distribution with mean zero and variance RT_T for the tangential components of molecular velocity and the one-dimensional Gauss distribution with mean zero and variance RT_L, as will be

[3] The mean free path is given by $\ell = m/(\sqrt{2}\pi d_m^2 \rho)$, Eq. (2.72) in Sect. 2.3.1.

[4] See Sect. 2.2.1.

explained in Chap. 2 [18]; the temperature T_T is a linear function of energy flux across the interface and T_L is the temperature of liquid. For the weak evaporation or condensation, T_T can be regarded to be approximately equal to T_L. The KBC has also a factor including the well-defined evaporation coefficient α_e and condensation coefficient α_c; α_e is identical with α_c in the equilibrium state. This KBC reduces to the conventional KBC in the limit of the equilibrium state, i.e., $T_T = T_L$, but it does not contain any arbitrary parameter unlike the conventional KBC. The authors should note that any KBC for an arbitrarily strong evaporation or condensation has not been derived so far and its formulation is a challenging future work.

There has been a long history over α_e and α_c since pioneering studies of Hertz [15] and Kundsen [19]. For reference, values of α_e and α_c of water vapor are shown in Table 1.1 for the α_e-values and Table 1.2 for the α_c-values; these tables are reproduced on the basis of data of α_e and α_c reported in Marek and Straub's paper [23]. The recent MD simulation has succeeded in the determination of

Table 1.1 The evaporation coefficient α_e of water

Year	Author(s)	α_e	Temperature(°C)
1925	Rideal	0.0037–0.0042	25–30
1931	Alty	0.0083–0.0155	5.9–32
1931	Alty and Nicoll	0.0156	12.1
1933	Alty	0.0289–0.0584	−7.5–25
1935	Alty and Mackay	0.0061–0.0392	10.3–32.6
1939	Baranaev	0.033–0.034	10–50
1940	Prüger	0.02	100
1953	Hammecke and Kappler	0.045	20
1954	Hickman	0.254–0.532	5.9–7.3
1954	Hickman and Torpey	0.0047	1.2
1955	Kappler	0.0992–0.1015	3.8–20.2
1959	Fuchs	0.03–0.034	20
1964	Campbell	0.0014–0.0122	44.6–83.0
1964	Delaney et al.	0.0336–0.0545	−0.8–4.1
1965	Mendelson and Yerazunis	0.0008–0.0038	38.9–78.3
1967	Maa	1	0.05
1969	Maa	1	0.8
1971	Cammenga et al.	0.002	24–30
1971	Cammenga et al.	0.248–0.380	18
1971	Duguid and Stampfer	0.5–1	25–35
1971	Tamir and Hasson	0.10–0.30	42–50
1973	Levine	1	20–28
1975	Davies et al.	1	4–19.5
1975	Kochurova et al.	0.050–0.065	25.5–34.5
1975	Narusawa and Springer	0.038	18–27
1975	Narusawa and Springer	0.19	18–27
1976	Bonacci et al.	0.065–0.665 (avg.0.54)	2.1–8.7
1978	Barnes	0.0002	25
1987	Čukanov	0.008–0.034	39.8
1989	Hagen et al.	0.13	16
2005	Ishiyama et al. (MD)	$\lesssim 1$	≈ 36

Table 1.2 The condensation coefficient α_c of water vapor

Year	Author(s)	α_c	Temperature(°C)
1961	Berman	1	10
1963	Nabavian and Bromley	0.35–1	7–50
1963	Wakeshima and Takata	0.015–0.020	−16.1–5.1
1964	Goldstein	≈ 0.1	25–30
1964	Jamieson	0.305	0–70
1965	Jamieson	0.35	–
1965	Tanner et al.	> 0.08	100
1967	Mills and Seban	0.45–1	7.6–10.2
1968	Tanner et al.	> 0.1	22–46
1969	Maa	1	0.8–8.2
1969	Wenzel	1.0	22–46
1971	Magal	0.040–0.044	25.9–82.8
1971	Tamir and Hasson	0.09–0.35	48.5–105.5
1973	Vietti and Schuster	0.21	–
1974	Chodes et al.	0.031–0.037	23.9–24.9
1974	Gollub et al.	0.010–0.012	11.4–17.5
1975	Sinnarwalla et al.	0.021–0.032	22.5–25.7
1975	Vietti and Fastook	1	20.8–23.2
1976	Vietti and Fastook	0.1–1	20
1976	Bonacci et al.	0.417–0.693	5.5–7.0
1976	Finkelstein and Tamir	0.006–0.060	60–99
1978	Neizvestnyj et al.	0.3–1	20
1986	Hatamiya and Tanaka	0.2–0.6	6.9–26.9
1987	Garnier et al.	0.01	$\approx$ 20–25
1989	Hagen et al.	0.01	16
2010	Fujikawa et al.	$\lesssim 1$	17–20

α_e-values for water [17] as shown in Table 1.1, although the simulation result is not yet verified by experiments. Concerning α_c, it had not been determined accurately before the authors' values in Table 1.2.[5] We can see that the values of α_e and α_c largely scatter in the range of more than one hundred times. In the next section, we will consider theoretically the reason why the determination of the values of α_e and α_c has been so difficult. Without reliable α_e and α_c-values, the KBC remains open for ever.

The establishment of the KBC allows us to derive a set of boundary conditions for the set of Navier–Stokes equations, i.e., a set of continuity, momentum, and energy equations in the local equilibrium region, fluid-dynamics region outside the Knudsen layer, by theoretical analysis of the Knudsen layer based on the Gaussian–BGK Boltzmann equation [1], as will be discussed in Chap. 2. The Gaussian–BGK Boltzmann equation is the only polyatomic version of the Boltzmann equation satisfying the H-theorem. For resolving the above-mentioned problems of α_e, α_c, and the boundary conditions for the set of Navier–Stokes equations, we have at present no any consistent law or any consistent system of governing equation. We have

[5] Fujikawa et al.'s experimental values are given in Fig. 3.24 in Sect. 3.6.5.

the only theoretical method and two kinds of governing equations, i.e., MD, the Gaussian–BGK Boltzmann equation, and the set of Navier–Stokes equations. In this book, matching among MD, the Gaussian–BGK Boltzmann equation, and the set of Navier–Stokes equations will be consistently done.

1.2 Why Are Measurements of α_e and α_c So Difficult?

In this section, we demonstrate that the difficulty in the measurement of α_e and α_c lies in the existence of different time scales essential for the phase change phenomena. This difficulty can be overcome by conducting the measurement of the condensation induced by an abrupt pressure elevation caused by the reflection of shock wave at the interface. We therefore start with the discussion of a shock reflection phenomenon.

1.2.1 Unsteady Nonequilibrium Condensation Induced by Shock Wave Reflection

As mentioned in Sect. 1.1, the α_e and α_c-values measured in the past largely scatter in the range of more than one hundred times. We will here discuss the reason why these values are so different in such a wide range. The determination of α_e or α_c must be made through the measurement of a small amount of net mass flux of the evaporation or condensation at the interface in a nonequilibrium state; the measurement is not feasible at the equilibrium state. Such a nonequilibrium state can be realized by the following way. Let us consider the situation where the half-infinite extent of a vapor is in contact with the half-infinite extent of the liquid phase of the vapor, and these are facing each other with the plane interface between and in an equilibrium state. As shown in Fig. 1.3, a shock wave advancing from the right-hand side in the vapor collides with the interface and it is reflected, and propagating in the right-hand direction as the time elapses; the time is running upward.

Just at the instant when the shock wave is reflected at the interface, the pressure, temperature, and density of the vapor increase stepwise from the initially low state to a high one. The temperature of the vapor at the interface changes little because of the large difference in heat capacities of the vapor and liquid. The Knudsen layer is formed near the interface in the vapor, and the thermal boundary layer also develops outside the Knudsen layer with the lapse of time. The vapor pressure at the interface then becomes higher than the saturated vapor pressure at the interfacial liquid temperature.

As a result, the vapor becomes supersaturated at the interface, consequently condensing, and the interface moves toward right-hand side with time. The net mass flux of condensation at the interface, which we need, can be obtained from the measurement of interface movement. This problem has been solved by Fujikawa et al. [10] for the system of shock tube endwall, liquid film, and vapor on the basis of the method of matched asymptotic expansions, as will be mentioned in Sect. 3.2.2;

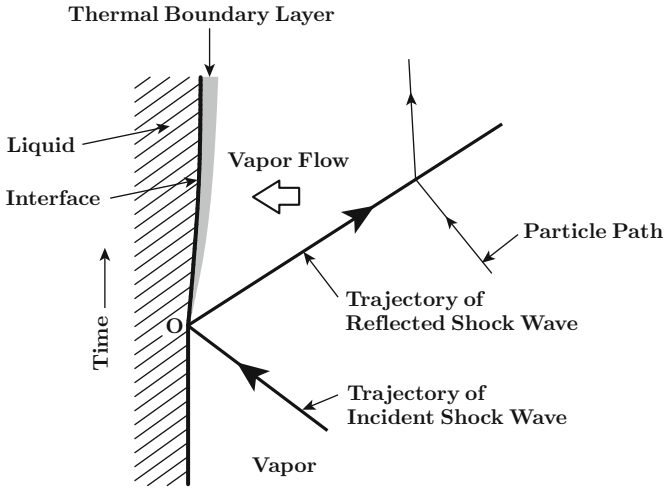

Fig. 1.3 The propagation process of the shock wave in the vapor advancing toward and reflecting from the liquid surface. The time is running upward

the reflection of a shock wave at the shock tube endwall in a noncondensable gas has been analyzed by Clarke [5]. The problem shown in Fig. 1.3 is a simplified version of Ref. [10] and the result of its analysis can be summarized as follows.

For simplicity, we will assume $\alpha = \alpha_e = \alpha_c$ and adopt a set of fluid-dynamic boundary conditions at the interface for the set of Navier–Stokes equations as follows [1, 28, 29][6]:

$$\frac{u}{\sqrt{2RT_L}} = \frac{p - p^*}{p^*} \frac{1}{C_4^* - 2\sqrt{\pi}\frac{1-\alpha}{\alpha}}, \tag{1.1}$$

$$\frac{T - T_L}{T_L} = d_4^* \frac{u}{\sqrt{2RT_L}}, \tag{1.2}$$

where T_L is the liquid temperature at the interface, T is the vapor temperature at the interface, p^* is the saturated vapor pressure at T_L, p is the vapor pressure at the interface, u is the vapor velocity at the interface, R is the gas constant per unit mass, and $C_4^* = -2.13204$ and $d_4^* = -0.44675$ for Boltzmann–Krook–Welander (BKW) model; C_4^* and d_4^* are slightly different among models such as BKW and

[6] This assumption holds for the weak evaporation or condensation which takes place near the equilibrium state, as will be discussed in Chaps. 2 and 3. Equations (1.1) and (1.2) are respectively Eqs. (2.138) and (2.139) in Sect. 2.5.3 for the case that the vapor flow is one-dimensional and the flow velocity is much larger than the moving velocity of the interface. And, also see Footnote 20 in Sect. 2.5.3.

hard-sphere models.[7] The more general boundary conditions for polyatomic gases will be given in Chap. 2 in this book, but Eqs. (1.1) and (1.2) suffice for the present purpose. Fujikawa et al. have solved the set of one-dimensional Navier–Stokes equations of vapor and the heat conduction equation of lquid together with Eqs. (1.1) and (1.2) by the method of matched asymptotic expansions [9, 10]. The time-dependent position $\delta(t)$ of the interface from its initial one is then described at the level of the first approximation by

$$\frac{\mathrm{d}\delta(t)}{\mathrm{d}t} = \frac{\sqrt{2RT_L(t)}}{\phi(\alpha)} \frac{\rho_\infty}{\rho_L} \frac{T_\infty}{T_L(t)} \frac{p_\infty - p^*(T_L)}{p^*(T_L)}, \tag{1.3}$$

$$T_L(t) = T_0 + \frac{\rho_L L}{k_L} \sqrt{\frac{D_L}{\pi}} \int_0^t \frac{\mathrm{d}\delta(\tilde{t})/\mathrm{d}\tilde{t}}{\sqrt{t-\tilde{t}}} \mathrm{d}\tilde{t}. \tag{1.4}$$

Here, t is the time measured from the instant of the step change of the state, T_0 is the initial temperature of the vapor and liquid, ρ_∞ and T_∞ are the vapor density and temperature far from the interface behind the reflected shock wave, ρ_L is the liquid density, D_L is the thermal diffusivity of liquid, k_L is the thermal conductivity of liquid, L is the latent heat of condensation, and $\phi(\alpha)$ and $p^*(T_L)$ are respectively given by

$$\phi(\alpha) = -C_4^* + 2\sqrt{\pi} \frac{1-\alpha}{\alpha}, \tag{1.5}$$

$$p^*(T_L) = p_0^* \left[1 - A + \frac{A}{T_0} T_L(t) \right], \tag{1.6}$$

where $p_0^* = p^*(T_0)$ and $A = bT_0/(c+T_0)^2$ in which b and c are given later [Eqs. (1.9) and (1.10)]; ρ_L, D_L, k_L, and L are constant values. Equation (1.6) is obtained from Antoine's equation [30] by Taylor's expansion, and $p^*(T_0) = p_0^*$ as it should be so; Antoine's equation is given below in Eq. (1.7).

The saturated vapor pressure p^* and the saturated vapor density ρ^* can be obtained by Antoine's equation and the state equation for ideal gases:

$$p^* = \exp\left(a - \frac{b}{c + T_L} \right), \tag{1.7}$$

$$\rho^* = \frac{p^*}{RT_L}, \tag{1.8}$$

[7] The values of C_4^* and d_4^* are given in Eq. (2.134) for hard-sphere gas and Eq. (2.136) for the BKW model.

where the units of T_L and p^* are respectively (K) and (Pa), and the constant values a, b, and c are for methanol vapor

$$a = 23.4803, \qquad b = 3626.55, \qquad c = -34.29, \tag{1.9}$$

and for water vapor

$$a = 23.1964, \qquad b = 3816.44, \qquad c = -46.13. \tag{1.10}$$

From Eqs. (1.3), (1.4), and (1.6), we obtain a Volterra integral equation of the second kind on the displacement speed of the interface as follows:

$$\frac{\mathrm{d}\delta(t)}{\mathrm{d}t} = \beta_1 - \frac{\beta_2}{\sqrt{\pi}} \int_0^t \frac{\mathrm{d}\delta(\tilde{t})/\mathrm{d}\tilde{t}}{\sqrt{t-\tilde{t}}} \mathrm{d}\tilde{t}, \tag{1.11}$$

where

$$\left.\begin{aligned} \beta_1 &= \frac{p_\infty (p_\infty - p_0^*)}{\phi(\alpha)\rho_L p_0^*} \sqrt{\frac{2}{RT_0}}, \\ \beta_2 &= \frac{p_\infty (p_\infty - p_0^* + 2Ap_\infty)L}{\phi(\alpha) k_L p_0^*} \sqrt{\frac{D_L}{2RT_0^3}}. \end{aligned}\right\} \tag{1.12}$$

The solution of Eq. (1.11) can be obtained as [6]

$$\frac{\mathrm{d}\delta(t)}{\mathrm{d}t} = \beta_1 \exp(\beta_2^2 t)\mathrm{erfc}(\beta_2\sqrt{t}), \tag{1.13}$$

where

$$\mathrm{erfc}(\beta_2\sqrt{t}) = \frac{2}{\sqrt{\pi}} \int_{\beta_2\sqrt{t}}^{\infty} e^{-x^2} \mathrm{d}x. \tag{1.14}$$

Integrating Eq. (1.13) with respect to the time t leads to

$$\delta(t) = \frac{\beta_1}{\beta_2^2} \left[\exp(\beta_2^2 t)\mathrm{erfc}(\beta_2\sqrt{t}) + \frac{2}{\sqrt{\pi}} \beta_2 \sqrt{t} - 1 \right]. \tag{1.15}$$

where $\delta(0) = 0$. From Eqs. (1.4), (1.11), and (1.13), we obtain

$$T_L(t) = T_0 + \frac{\beta_1 \rho_L L \sqrt{D_L}}{\beta_2 k_L} \left[1 - \exp(\beta_2^2 t)\mathrm{erfc}(\beta_2\sqrt{t}) \right]. \tag{1.16}$$

where $T_L(0) = T_0$. The position and temperature of the interface are respectively described by Eqs. (1.15) and (1.16).

1.2.2 Temporal Transition Phenomenon of Interface Displacement

Equations (1.15) and (1.16) can be classified into two cases depending on values of the variable $\beta_2\sqrt{t}$ as follows:

(1) for $\beta_2\sqrt{t} \ll 1$[8];

$$\delta(t) = \beta_1 t, \tag{1.17}$$

$$T_L(t) = T_0 + \frac{2\beta_1\rho_L L}{k_L}\sqrt{\frac{D_L}{\pi}t}, \tag{1.18}$$

(2) for $\beta_2\sqrt{t} \gg 1$[9];

$$\delta(t) = \frac{2}{\sqrt{\pi}}\frac{\beta_1}{\beta_2}\sqrt{t} - \frac{\beta_1}{\beta_2^2}, \tag{1.19}$$

$$T_L = T_0 + \frac{\rho_L L\sqrt{D_L}}{k_L}\frac{\beta_1}{\beta_2}(= \text{const.}), \tag{1.20}$$

where we should notice, for the following discussion, that β_1 and β_1/β_2^2 are dependent on $\phi(\alpha)$, i.e., α, while β_1/β_2 is independent of $\phi(\alpha)$. The displacement of the interface is drastically influenced by $\phi(\alpha)$ and the time measured from the instant of the step change of the state. For $\beta_2\sqrt{t} \ll 1$, the position of the interface changes in proportion to the time and the interface speed depends on $\phi(\alpha)$, while for $\beta_2\sqrt{t} \gg 1$ the position changes in proportion to the square root of the time, and its change gradually becomes independent of $\phi(\alpha)$ as the time lapse and becomes strongly dependent on thermophysical properties of the vapor and liquid. This suggests that the position of the interface should be measured in early time stages just after the

---

[8] For small values of x, erfc x can be expressed as follows [3]:

$$\text{erfc}\, x = 1 - \text{erf}\, x = 1 - \frac{2}{\sqrt{\pi}}\sum_{n=0}^{\infty}\frac{(-1)^n x^{2n+1}}{(2n+1)n!},$$

where erf x is the error function.

[9] For large values of x, erfc x can be expressed as follows [3]:

$$\frac{\sqrt{\pi}}{2}\text{erfc}\, x = \int_x^{\infty} e^{-\xi^2}\mathrm{d}\xi = \frac{1}{2}e^{-x^2}\left[\frac{1}{x} - \frac{1}{2x^3} + \frac{1.3}{2^2x^5} - \cdots + (-1)^{n-1}\frac{1.3\ldots(2n-3)}{2^{n-1}x^{2n-1}}\right]$$
$$+ (-1)^n\frac{1.3\ldots(2n-1)}{2^n}\int_x^{\infty}\frac{e^{-\xi^2}\mathrm{d}\xi}{\xi^{2n}}.$$

step change caused by the shock reflection, when we determine α through the measurement of the interface displacement.

It is quite natural to notice, in the above discussion, that there exists a transition time between the t-proportion displacement of the interface and the $\sqrt{t}$-proportion one and that this time can be deduced from the relation $\beta_2\sqrt{t} = O(1)$. Defining the transition time as τ_t when $\beta_2\sqrt{\tau_t} = 1$, we obtain

$$\tau_t = \frac{2RT_0^3}{D_L}\left[\frac{\phi(\alpha)k_L p_0^*}{p_\infty(p_\infty - p_0^* + 2Ap_\infty)L}\right]^2. \tag{1.21}$$

The transition time τ_t is in proportion to $[\phi(\alpha)]^2$. Generally, $\phi(\alpha)$ approaches $-C_4^*$ ($= 2.13204$ for hard-sphere gas) as α does unity, and on the other hand, $\phi(\alpha)$ approaches infinity as α does zero. Evaluating τ_t for small pressure changes by 5 % from the saturated vapor pressures at 290 K for methanol and water vapors, we obtain, e.g., for $\alpha = 1$, $\tau_t \cong 0.1$ μs for methanol vapor and $\tau_t \cong 7$ μs for water vapor, respectively. In both cases, the transition times are very short. The reason why the transition time of methanol vapor is shorter than that of water vapor is principally because the saturated vapor pressure of methanol is six times higher than that of water at 290 K; the vapor with the higher saturated pressure causes the more mass flux and the more rapid temperature rise of liquid, thereby resulting in the shorter transition time.

If the liquid is a very thin film and it is on a solid wall with a thermal conductivity higher than that of the liquid, the transition time becomes a little longer (see Sect. 3.2.2). Although the restriction of transition time for the measurement of interface displacement is not so strict, we can understand that the measurement should be carried out in the time scale of microseconds, not in time scale of milliseconds or seconds. All values of α_e and α_c shown in Tables 1.1 and 1.2 have been measured in the past through the displacement of plane or curved liquid surface directly, or other indirect ways. However, there was no recognition of the existence of the temporal transition phenomenon in the past measurements. This is one of reasons why the values of α_e and α_c measured have been largely different.

1.2.3 Mechanism of Temporal Transition Phenomenon

As clarified in the preceding subsection, the displacement of the interface greatly depends on the change of the saturated vapor pressure at the interfacial liquid temperature. The time evolution of the temperature is given by Eq. (1.18) for $t \ll \tau_t$ and by Eq. (1.20) for $t \gg \tau_t$. The temperature at the time τ_t is given by

$$T_L = T_0 + 0.5724\frac{\beta_1\rho_L L\sqrt{D_L}}{\beta_2 k_L}. \tag{1.22}$$

At this time stage, the temperature rise is about 57% of the temperature variation from its initial value to the asymptote [$= \beta_1 \rho_L L \sqrt{D_L}/(\beta_2 k_L)$]. Therefore, we can understand that the transition time is the characteristic time when the temperature approaches the asymptote over the time.

Now, let us consider the balance of heat fluxes at the interface in order to understand the mechanism of the temporal transition phenomenon. The balance equation of heat fluxes per unit time and unit interface area is given by

$$\left.\begin{aligned} \rho_L L \frac{\mathrm{d}\delta(t)}{\mathrm{d}t} &\cong \text{heat conduction into liquid} \\ &\propto \frac{T_L(t) - T_0}{\sqrt{t}}, \end{aligned}\right\} \tag{1.23}$$

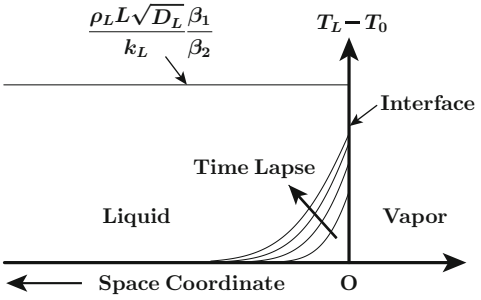

(a) Before Transition Time

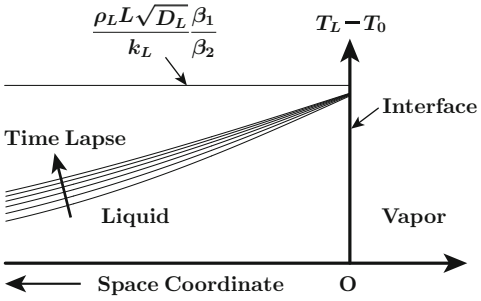

(b) After Transition Time

Fig. 1.4 Temperature changes of liquid surface and liquid interior: (**a**) before transition time and (**b**) after transition time